A Novel Actuator Controller: Delivering a Practical Solution to Realization of Active-Truss-Based Morphing Wings

Difan Tang, *Student Member*, *IEEE*, Lei Chen, *Member*, *IEEE*, Eric Hu, and Zhao F. Tian

***Abstract*—A novel actuator controller is proposed in this paper for active-truss-based morphing wings (ATBMWs). An ATBMW is a new type of smart structure capable of smooth and continuous profile change, and has the potential to provide better stealth and aerodynamic performance over airfoils with discrete control surfaces. However, the sophisticated ATBMW framework and large amount of highly interacted actuators make it difficult to obtain the overall rigid-body dynamics of the wing for controller design and inconvenient to tune controllers on board. The focus of this study is thus to solve the aforementioned problems by developing an actuator-level control scheme that does not rely on the wing rigid-body dynamics and on-board tuning. The linear-quadratic-Gaussian (LQG) controller is adopted for actuator trajectory tracking, and a novel unknown-input estimator (UIE) is devised to handle un-modeled dynamics. By integrating the UIE with the LQG algorithm, a new tracking controller with enhanced tolerance to uncertainties is constructed. It is shown in simulations and experiments on an ATBMW prototype that the proposed UIE-integrated LQG controller can be designed simply using the known actuator dynamics without on-board tuning, and superior trajectory tracking of actuators was observed despite the presence of un-modeled dynamics and exogenous disturbances.**

***Index Terms*—Disturbance rejection, model error compensation, morphing wing, motion control, tracking control, unknown-input estimation.**

I. Introduction

DURING flight, the profile variation of airfoils not only affects aircraft maneuver but also contributes to energy efficiency under different conditions [1]. As one of the various morphing wing technologies, the active-truss-based morphing wing (ATBMW) is believed to have better stealth and aerodynamic performance over airfoils with discrete control surfaces commonly seen on modern aircraft [2]. An ATBMW can make large shape change while keeping the wing profile smooth and continuous in the meantime (i.e. shape morphing). This is achieved through truss structures that use embedded actuators as active elements. Altering the length of the active truss struts can change the shape of an ATBMW while the overall structure integrity and strength are maintained [2]–[4].

However, difficulties in modeling and on-board tuning have made conventional methods of actuator control inapplicable to ATBMWs (see Section II). Satisfactory solutions to these problems, although of vital importance to successful realization of the promising ATBMW concept on aircraft, have nevertheless received little research attention. An approach bypassing the necessity of obtaining the wing rigid-body dynamics and on-board tuning is thus proposed in this paper.

The key point of our proposed solution lies in the development of a new unknown-input estimation scheme to handle un-modeled dynamics. Exogenous disturbances can also be effectively treated under the same scheme. In reality, a control system is always subjected to unknown inputs in the form of internal uncertainties (i.e. un-modeled dynamics) and exogenous loads that are not measurable or are inconvenient to measure. If these unknown inputs are not properly treated, poor performance of the control system may result. To attenuate the negative impact from unknown inputs, various methods can be used. A common practice is to maximize the inherited robustness of a controller by careful parameter design and tuning [5], [6]. Further robustness improvement can be achieved via advanced techniques such as nonlinear control [7]–[9], H_∞ or optimized loop-shaping robust control [10]–[12], and adaptive intelligent control [13], [14]. A more attractive approach distinguished from the aforementioned comes with the concept of unknown-input estimation, which brings disturbance rejection to a higher level, as demonstrated by various industrial applications [15]–[22]. This technique provides the controller with better tolerance to uncertainties by constructing counteractive control efforts to cancel the effects from unknown inputs according to real-time estimation.

The use of an extended state observer [21], [23] or the internal model principle [12], [24] can effectively estimate a class of partially unknown inputs modeled in the form of constant-coefficient differential equations. A prerequisite is that characteristics of the exogenous inputs such as the frequency of each sinusoidal component must be known. When only the order of the exogenous inputs is known and these disturbances perturb the system through channels other than those of the control inputs, a generalized extended state observer can be used [25]–[27]. For systems with nonlinear modeling, nonlinear disturbance observers are also available [28], [29]. However, higher-order observers are required when dealing

Manuscript received August 23, 2015; revised January 4, 2016 and March 28, 2016; accepted May 1, 2016. Research undertaken for this paper has been assisted by a grant from the Sir Ross and Sir Keith Smith Fund (Smith Fund) (www.smithfund.org.au). The support is acknowledged and greatly appreciated.

D. Tang, L. Chen, E. Hu, and Z. F. Tian are with the School of Mechanical Engineering, the University of Adelaide, Adelaide, SA 5005, Australia (e-mail: difan.tang@adelaide.edu.au; lei.chen@adelaide.edu.au; eric.hu@adelaide.edu.au; zhao.tian@adelaide.edu.au).

with complex disturbing exogenous inputs, and this increases the observer dimension as a result. Estimating completely unknown inputs is possible by combining an observer with an additional estimation function. Some early work require to decouple unknown-input estimation from state estimation [30], while most later studies do not, in which an ordinary state observer [31] can still work properly under the situation that the unknown inputs are canceled by corresponding control inputs. Using a reference model [32] directly together with an estimation function is able to do a similar job. Among these studies, other limitations arise. Some methods require the derivatives of measured outputs [19], [32], which make the estimation sensitive to noises or modeling errors; Some rank conditions apply to unknown inputs in the work of [33], [34], and [35]; The complexity of parameter selection rises due to the less restrictive conditions on unknown inputs [20], [22], [35]–[37]; In [38], [39] the state observer gain is constrained by the estimation scheme of unknown inputs, and limited design freedom is given to unknown-input estimation as well. As a counterpart of design in the state space, the disturbance observer (DOB) synthesized in the frequency domain relies on a customized low-pass filter and the inversion of plant dynamics [40]–[43]. The custom low-pass filter design, which influences the stability of the plant, can be intricate when an optimal set of filter coefficients are desired through an optimization procedure. The plant inversion also causes some difficulties in employing DOBs in multi-input multi-output (MIMO) systems since an inverse cannot always be found. The generalization of the DOB to MIMO cases bypasses the plant inversion and adopts parameterized controller design through an optimization process [44], [45]. Nevertheless, the global optimum is hard to guaranteed in these methods.

The aforementioned studies in terms of unknown-input estimation each suits some particular industrial application(s), but are not the ideal candidate for the ATBMW application due to the mentioned limitations. The work in this paper therefore aims to solve the actuator control problems that are hindering the realization of ATBMWs, by developing a robust actuator-level control scheme with a new unknown-input estimation method. Major contributions are as follows:

Firstly, a new approach for unknown-input estimation exempted from the aforementioned limitations is devised.

Secondly, the new unknown-input estimation scheme is integrated into a linear-quadratic-Gaussian (LQG) servo controller so that the wing rigid-body dynamics is not required for the controller design and on-board tuning is not needed. To the best of our knowledge, the resulting new control scheme is the first successful approach practically solving the actuator control problem associated with ATBMW applications, pioneering the realization of the promising ATBMW concept.

To avoid confusion and for unity, the scheme for unknown-input estimation in this paper is termed as 'unknown-input estimator' (UIE).

II. Active-Truss-Based Morphing Wing

A. Challenges in Control and Proposed Solution

Advanced ATBMWs generally need more actuators for more flexible shape morphing and better aerodynamic performance, and adjacent actuators in most cases are mechanically coupled and mutually constrained as in [2], [3]. The sophisticated ATBMW frameworks and the large amount of highly interacted actuators cause considerable difficulties in analytically, numerically, and experimentally acquiring the dynamic model of the entire wing structure and in performing on-board tuning of controllers. These make the implementation of centralized MIMO control difficult.

To deliver a practical solution to the realization of the concept of ATBMW, this paper therefore proposes an approach bypassing the necessity of obtaining the wing rigid-body dynamics and on-board tuning. To do so, each actuator is assigned an individual controller, the design of which is desired to be purely based on the dynamics of the actuator (readily available), without impairing prescribed performance. However, as adjacent actuators in most cases are mechanically coupled and mutually constrained, the wing rigid-body dynamics distributed at each actuator are coupled. In addition, other various induced forces such as the inertia loads of the framework, the frictions in joints and between sliding wing skin layers, and the resistance from elastic skin deformation also have an impact on actuator performance. To solve these problems, the coupled and other forms of un-modeled dynamics are treated together as an equivalent unknown input, estimated, and canceled by introducing an unknown-input estimator, as detailed in Section III. In this case, actuator controllers can be tested and tuned before the actuators are assembled onto the wing, and on-board tuning is thus no longer needed. Depending on the input-output configuration of the actuator, it is possible to further reduce the control problem to a set of single-input single-output (SISO) cases, which significantly simplifies the overall implementation.

B. ATBMW Prototype

To experimentally validate the proposed method for delivering a practical solution to the realization of the ATBMW concept, an ATBMW prototype was developed. The prototype has a specially simplified truss configuration at the cost of sacrificing aerodynamic performance to allow identification of wing rigid-body dynamics distributed at each actuator. In practice, functional ATBMWs can have many variations, requiring increased complexity in terms of truss configuration.

The section view of the prototype is shown in Fig. 1, where nodes are denoted by numbers while struts are labeled with letters. Any strut can be active, but in this prototype only struts B, L, M, N, and O are each embedded with an electric ball-screw miniature linear actuator due to size limit (actuators mentioned hereinafter are named the same as active struts). Nodes 1, 2, 5, and 6 are fixed so that the framework can be fixed to the spar. The wing skin is constructed by layers of sliding aluminum sheets of 0.1mm thick. The whole wing section has a chord length of 591mm at zero camber, a maximum thickness of 71mm at 30% of chord from the leading edge, and a span of 150mm.

Dynamic models for controller design were acquired via system identification, with voltages (V) as inputs and displacements (mm) as outputs. The iterative prediction-error

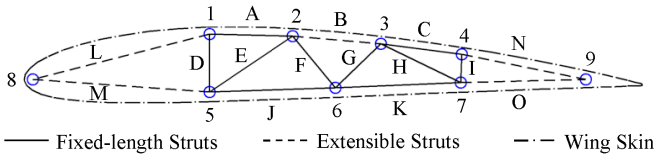

Fig. 1. Schematic of the ATBMW prototype structural configuration.

TABLE I
EXPERIMENTALLY IDENTIFIED DYNAMICS

Active Struts	Matrices of System Dynamics[a]			
	Category I		Category II	
	$\boldsymbol{A}_I$	$\boldsymbol{B}_I$	$\boldsymbol{A}_{II}$	$\boldsymbol{B}_{II}$
B	$\begin{bmatrix} 0 & 1 \\ 0.0006 & -14.75 \end{bmatrix}$	$\begin{bmatrix} 0.099 \\ 11.36 \end{bmatrix}$	$\begin{bmatrix} 0 & 1 \\ 5.49 & -59.61 \end{bmatrix}$	$\begin{bmatrix} 0.113 \\ 26.70 \end{bmatrix}$
L	$\begin{bmatrix} 0 & 1 \\ 0.0251 & -24.85 \end{bmatrix}$	$\begin{bmatrix} 0.036 \\ 25.27 \end{bmatrix}$	$\begin{bmatrix} 0 & 1 \\ 3.34 & -56.18 \end{bmatrix}$	$\begin{bmatrix} 0.048 \\ 47.08 \end{bmatrix}$
M	$\begin{bmatrix} 0 & 1 \\ 0.0455 & -23.65 \end{bmatrix}$	$\begin{bmatrix} 0.032 \\ 19.11 \end{bmatrix}$	$\begin{bmatrix} 0 & 1 \\ 2.35 & -40.27 \end{bmatrix}$	$\begin{bmatrix} 0.007 \\ 31.53 \end{bmatrix}$
N	$\begin{bmatrix} 0 & 1 \\ 0.4543 & -27.95 \end{bmatrix}$	$\begin{bmatrix} 0.138 \\ 23.39 \end{bmatrix}$	$\begin{bmatrix} 0 & 1 \\ 0.37 & -39.34 \end{bmatrix}$	$\begin{bmatrix} 0.004 \\ 24.40 \end{bmatrix}$
O	$\begin{bmatrix} 0 & 1 \\ 0.3867 & -16.99 \end{bmatrix}$	$\begin{bmatrix} 0.217 \\ 11.39 \end{bmatrix}$	$\begin{bmatrix} 0 & 1 \\ 0.15 & -19.33 \end{bmatrix}$	$\begin{bmatrix} 0.200 \\ 8.55 \end{bmatrix}$

[a] For both categories, $\boldsymbol{C}_I = \boldsymbol{C}_{II} = [1 \quad 0]$ and $\boldsymbol{D}_I = \boldsymbol{D}_{II} = 0$.

minimization method [46] is used to estimate the black-box state-space model in the form of

$$\begin{cases} \dot{\boldsymbol{x}}(t) = \boldsymbol{A}\boldsymbol{x}(t) + \boldsymbol{B}\boldsymbol{u}(t) \\ \boldsymbol{y}(t) = \boldsymbol{C}\boldsymbol{x}(t) + \boldsymbol{D}\boldsymbol{u}(t) \end{cases}, \tag{1}$$

where $\boldsymbol{x}(t) \in \mathbb{R}^{n_x}$, $\boldsymbol{y}(t) \in \mathbb{R}^{n_y}$, and $\boldsymbol{u}(t) \in \mathbb{R}^{n_u}$ are vectors of n_x system states, n_y measured outputs, and n_u control inputs, respectively; $\boldsymbol{A} \in \mathbb{R}^{n_x \times n_x}$, $\boldsymbol{B} \in \mathbb{R}^{n_x \times n_u}$, $\boldsymbol{C} \in \mathbb{R}^{n_y \times n_x}$, and $\boldsymbol{D} \in \mathbb{R}^{n_y \times n_u}$ are system matrices of appropriate dimensions.

For comparison, two categories of models were obtained (Table. I). Models in *Category I* are the dynamics of individual actuators, identified separately for each single actuator when the actuator was detached from the wing. As a special treatment in our proposed method as discussed at the beginning of this section in order to deliver a practical solution to the realization of the ATBMW concept, these models are used as the nominal system dynamics for controller design. Models in *Category II* describe the wing rigid-body dynamics distributed at each actuator. These models were identified when actuators were mounted on the wing, and hence contain the information of various induced forces (e.g. the inertia loads of the framework, the frictions in joints and between sliding wing skin layers, the resistance from elastic skin deformation, etc.). As demonstrated later in simulations in Section IV, these models are used to represent the actual system dynamics. It is worth noting that the wing prototype was specially designed to have the simplest functional truss structure so that Category II models could be identified for comparison. For more complicated configurations as in [3] the rigid-body dynamics of the entire wing structure are much more difficult to obtain.

The identified models are linear and time-invariant, which are desired for ease in controller design using well-established methods. Modeling errors inevitably exist due to the nonlinearities and uncertainty that are present in an actual system. This means, when only the actuator dynamics are used for controller design, the controller on an ATBMW is expected to cope with not only un-modeled wing rigid-body dynamics and exogenous disturbances but also the modeling errors in terms of the actuator dynamics per se.

III. ACTUATOR CONTROLLER

A. Problem Statements and Assumptions

Actuator-level control is discussed herein. It is a tracking problem in which the extension (the axial displacement of the moving rod) of each actuator should follow the reference length specified in real time. Each actuator has an individual controller, with the extension of actuators measured and fed back, and hence the actuator control problem is reduced to an SISO case.

The general plant model to be considered is given by

$$\begin{cases} \dot{\boldsymbol{x}}(t) = \boldsymbol{A}\boldsymbol{x}(t) + \boldsymbol{B}u(t) + \boldsymbol{B}_d\boldsymbol{d}(t, \boldsymbol{x}, \boldsymbol{\psi}) \\ y(t) = \boldsymbol{C}\boldsymbol{x}(t) \end{cases}, \tag{2}$$

where $u(t)$, $y(t)$, $\boldsymbol{x}(t)$, $\boldsymbol{A}$, $\boldsymbol{B}$, and $\boldsymbol{C}$ are defined the same as in (1); $\boldsymbol{d}(t, \boldsymbol{x}, \boldsymbol{\psi}) \in \mathbb{R}^{n_d}$ is a vector of n_d unknown inputs that the system is subjected to, including uncertain, nonlinear, time-varying, and state-dependent terms, with $\boldsymbol{\psi}$ denoting the arguments of nonlinear functions; $\boldsymbol{B}_d \in \mathbb{R}^{n_x \times n_d}$ is the distribution matrix of the unknown inputs.

The following assumptions are made:

Assumption 1: $(\boldsymbol{A}, \boldsymbol{B})$ is controllable.

Assumption 2: $(\boldsymbol{C}, \boldsymbol{A})$ is observable.

Assumption 3: $(\boldsymbol{A}, \boldsymbol{B}, \boldsymbol{C})$ has no zeros on the imaginary axis.

Assumptions 1 and 2 are basic requirements (from the state-space design perspective) for a plant to be properly controlled, and hold true for a majority of control systems (some systems may be partially controllable and observable). Assumption 3 is a condition for minimizing steady-state tracking errors and is naturally satisfied in systems involved in industrial applications requiring high-precision tracking [47].

Note that $\boldsymbol{B}_d$ can be either known or unknown, with no rank condition required, and there is no restriction on the number of unknown inputs $\boldsymbol{d}(t, \boldsymbol{x}, \boldsymbol{\psi})$. According to [38], an equivalent quantity exists at the control input channel which can replace the unknown inputs $\boldsymbol{d}(t, \boldsymbol{x}, \boldsymbol{\psi})$ in (2) under Assumptions 1 to 2. For simplicity and notation convenience, $\boldsymbol{d}(t, \boldsymbol{x}, \boldsymbol{\psi})$ is written as $\boldsymbol{d}(t)$ thereinafter, with t distinguishing the time-domain expression from frequency domain. Denote the equivalent unknown input by $d_e(t)$, and then (2) can be expressed as

$$\begin{cases} \dot{\boldsymbol{x}}(t) = \boldsymbol{A}\boldsymbol{x}(t) + \boldsymbol{B}\left[u(t) + d_e(t)\right] \\ y(t) = \boldsymbol{C}\boldsymbol{x}(t) \end{cases}. \tag{3}$$

As a result, we are able to use (3) as an equivalent of (2), and the control problem at this point is to estimate and feed back $d_e(t)$ to cancel $\boldsymbol{d}(t)$ so that satisfactory tracking performance can be maintained in the presence of modeling uncertainty and exogenous disturbances.

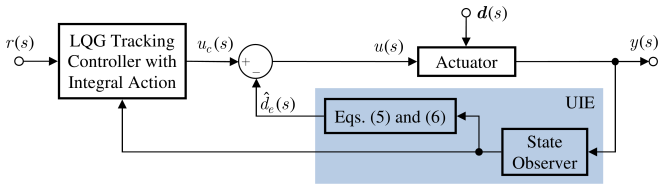

Fig. 2. Schematic of the proposed controller.

B. Controller Structure

The control scheme proposed in this paper is illustrated in Fig. 2. The LQG algorithm with integral action serves as the nominal tracking controller. Estimation and compensation of unknown inputs are integrated into the feedback loop in the form of a UIE component (the blue rectangle in Fig. 2).

In order to cancel the effects from unknown inputs $\boldsymbol{d}(t)$, or equivalently, $d_e(t)$, the control input $u(t)$ is defined as

$$u(t) = u_c(t) - \hat{d}_e(t), \tag{4}$$

where $u_c(t)$ is the normal control effort from the LQG component to realize prescribed actuator motion when there are no disturbing inputs $\boldsymbol{d}(t)$, and $\hat{d}_e(t)$ is an estimate of the equivalent unknown input.

Now we construct $\hat{d}_e(t)$ in the following form:

$$\hat{d}_e(t) = \hat{d}_{ev}(t) + K_d\left[y(t) - \hat{y}(t)\right], \tag{5}$$

where $\hat{d}_{ev}(t)$ is an adaptive auxiliary variable for estimating the equivalent unknown input, K_d is an estimation gain, and $\hat{y}(t)$ is an estimate of the plant output.

The auxiliary variable $\hat{d}_{ev}(t)$ is obtained and updated in real time via a subsystem $(\boldsymbol{A}_f, \boldsymbol{B}_f, \boldsymbol{C}_f)$ of n_f states with $\hat{d}_e(t)$ as the input:

$$\begin{cases} \dot{\boldsymbol{x}}_f(t) = \boldsymbol{A}_f\boldsymbol{x}_f(t) + \boldsymbol{B}_f\hat{d}_e(t) \\ \hat{d}_{ev}(t) = \boldsymbol{C}_f\boldsymbol{x}_f(t) \end{cases}, \tag{6}$$

where $\boldsymbol{A}_f \in \mathbb{R}^{n_f\times n_f}$, $\boldsymbol{B}_f \in \mathbb{R}^{n_f\times 1}$, and $\boldsymbol{C}_f \in \mathbb{R}^{1\times n_f}$ are system matrices.

Note that (6) only gives a general input-output form of the subsystem. In addition, $\boldsymbol{x}_f(t)$ do not have any direct physical implication in this general form, and n_f depends on the detailed structure of the subsystem. The design of $(\boldsymbol{A}_f, \boldsymbol{B}_f, \boldsymbol{C}_f)$ is flexible, and proper selection of the structure and parameters for the subsystem is addressed in detail in Sections III.C and III.D for ease of discussion.

To obtain the estimated plant output $\hat{y}(t)$, a state observer that takes $d_e(t)$ into account is needed and constructed as

$$\begin{cases} \dot{\hat{\boldsymbol{x}}}(t) = \boldsymbol{A}\hat{\boldsymbol{x}}(t) + \boldsymbol{B}[u(t) + \hat{d}_e(t)] + \boldsymbol{L}[y(t) - \hat{y}(t)] \\ \hat{y}(t) = \boldsymbol{C}\hat{\boldsymbol{x}}(t) \end{cases}, \tag{7}$$

where $\boldsymbol{L} \in \mathbb{R}^{n_x\times 1}$ is the estimation gain matrix of the state observer, and $\hat{\boldsymbol{x}}(t)$ is the estimate of the plant states.

Substituting $u(t)$ in (7) yields

$$\begin{cases} \dot{\hat{\boldsymbol{x}}}(t) = \boldsymbol{A}\hat{\boldsymbol{x}}(t) + \boldsymbol{B}u_c(t) + \boldsymbol{L}[y(t) - \hat{y}(t)] \\ \hat{y}(t) = \boldsymbol{C}\hat{\boldsymbol{x}}(t) \end{cases}. \tag{8}$$

Note that (8) is a standard form of the state observer in an LQG controller. Hence, the UIE can share the same state observer with the LQG controller.

The inclusion of a UIE in an LQG controller results in the control effort given by (4). To obtain $u_c(t)$, standard LQG design procedures [48] can be followed, assuming proper cancellation of unknown inputs by $\hat{d}_e(t)$.

Denote the target extension of an actuator by $r(t)$ and let

$$\dot{x}_w(t) = r(t) - y(t) = r(t) - \boldsymbol{C}\boldsymbol{x}(t). \tag{9}$$

Then the control effort from the LQG controller is

$$u_c(t) = -\boldsymbol{K}_x\hat{\boldsymbol{x}}(t) - K_w x_w(t) + K_r r(t), \tag{10}$$

where $\boldsymbol{K}_x$, K_w, and K_r are gains for the proportional state feedback, the integral action, and the feed-forward proportional term, respectively.

C. Closed-loop Analysis

Let $P_n(s)$, $G_d(s)$, $G_f(s)$, and $H(s)$ denote the transfer function of the input/output pairs $u(s) \to y(s)$, $d_e(s) \to y(s)$, $\hat{d}_e(s) \to \hat{d}_{ev}(s)$, and $y(s) \to u(s)$, respectively. With a UIE integrated, the following theorem on closed-loop stability and compensation of unknown inputs (including un-modeled dynamics and exogenous disturbances) holds.

Theorem 1: If a system as in (2) with any initial condition $\boldsymbol{x}(t_0)$ under Assumptions 1 to 3 is stabilized with full-state feedback (without a state observer and UIE) when $\boldsymbol{d}(\cdot) = 0$, then the system remains stable with the new control law as in (4) when subjected to any unknown inputs $\boldsymbol{d}(\cdot) \in \mathbb{R}^{n_d}$ of frequencies over the range of $\Omega \in [0,\ \omega_c]$ including un-modeled dynamics $M(s)$, given that the following conditions are satisfied:

(a) $1 - |G_f(j\omega)| \le \varepsilon_1$ for $\omega \in [0,\ \omega_c]$, $\forall \varepsilon_1 \in \mathbb{R}^+ \ll 1$.
(b) $\boldsymbol{L} \in \mathbb{R}^{n_x\times 1}$ and $K_d \in \mathbb{R}^+$ are selected such that $(\boldsymbol{A} - \boldsymbol{L}\boldsymbol{C} - \boldsymbol{B}K_d\boldsymbol{C})$ is stable, and

$$|M(j\omega)| < \left|1 + \frac{1}{H(j\omega)P_n(j\omega)}\right|,\ \forall\omega \in [0, +\infty). \tag{11}$$

Meanwhile for the input-output pair $y(j\omega) = G_d(j\omega)d_e(j\omega)$, the output $y(j\omega) \approx 0$ for $\omega \in [0,\ \omega_c]$, with the properly determined $\boldsymbol{K}_d \neq 0$.

Proof: See Appendix A. ■

Remark 1: The separation principle still holds for the full-state feedback and state observer design despite the inclusion of the UIE (as indicated by the closed-loop dynamics in (A.11) in Appendix A).

Remark 2: The dynamics of state estimation is given by:

$$\dot{\boldsymbol{e}}_x(t) = (\boldsymbol{A} - \boldsymbol{L}\boldsymbol{C})\,\boldsymbol{e}_x(t) + \boldsymbol{B}\xi(t), \tag{12}$$

where $\xi(t) = d_e(t) - \hat{d}_e(t)$. As shown in (12), the accuracy of state estimation is affected by the magnitude of $\xi(\cdot)$, and hence depends on the performance of the proposed UIE. Since fast and accurate estimation of $d_e(\cdot)$ is provided by the UIE according to Theorem 1, quick convergence of $\xi(t) \to 0$ is guaranteed. As a result, state estimation errors are subjected only to negligible residual equivalent unknown input. In other

words, the advantage of integrating a UIE into an existing LQG controller is that, it enables better state estimation performance in the presence of unknown inputs which are non-Gaussian, and meanwhile retains the merits of an optimal state observer in terms of sensor noise filtering.

Remark 3: Unlike the scheme in [38] and [39], the state observer design in our approach is not constrained by the UIE. This is because an additional parameter K_d is introduced, which gives a second degree of freedom in the UIE design.

Remark 4: As a new approach for estimating and compensating unknown inputs, the proposed UIE component integrated with the LQG controller works in a way that does not require detailed knowledge of unknown inputs, derivatives of measured outputs, inversion of plant dynamics, and parameter optimization for stabilizing purpose.

D. Controller Parameters Selection

As shown in Theorem 1, the design of the full-state feedback control law is independent of the UIE and can be conducted separately prior to the UIE design. Given that the design procedures for the optimal full-state feedback control are well established in literature, corresponding details are not repeated herein. In this subsection, guidelines for selecting parameters associated with the UIE are given. These parameters include the state observer gain $\boldsymbol{L}$, the UIE gain K_d, and the subsystem $(\boldsymbol{A}_f, \boldsymbol{B}_f, \boldsymbol{C}_f)$ or $G_f(s)$.

On the design of the subsystem $(\boldsymbol{A}_f, \boldsymbol{B}_f, \boldsymbol{C}_f)$, condition (a) is to be satisfied, and a low-pass filter with a unity passband gain is an ideal candidate (see Appendix A). Selection of ω_c is straightforward according to Theorem 1. With regard to the structure of $(\boldsymbol{A}_f, \boldsymbol{B}_f, \boldsymbol{C}_f)$, a 1^{st}-order low-pass filter can be used for its simplicity, least phase lag, and the significantly reduced system sensitivity it contributes to. Higher-order low-pass filter can also be considered. Exact knowledge regarding unknown inputs is normally unknown, it is thus a significant merit of the proposed UIE that selecting only one parameter, ω_c, can effectively treat a wide range of unknown inputs in a unified way, instead of determining the natural frequency of every possible unknown input individually.

The state observer shared by the LQG controller and the UIE component has limited effect in reducing the system sensitivity to unknown inputs (see Appendix A). Therefore, $\boldsymbol{L}$ can be selected normally for the LQG controller, and is not constrained by the UIE.

For selecting K_d, a systematic method based on linear-quadratic optimization is formulated as follows on an MIMO basis without losing generality.

The dynamics of state estimation is given by

$$\begin{cases} \dot{\boldsymbol{e}}_x(t) = (\boldsymbol{A} - \boldsymbol{LC})\boldsymbol{e}_x(t) - \boldsymbol{BK}_d\boldsymbol{C}\boldsymbol{e}_x(t) + \boldsymbol{\xi}'(t) \\ \boldsymbol{e}_y(t) = \boldsymbol{C}\boldsymbol{e}_x(t) \end{cases}, \quad (13)$$

where $\boldsymbol{e}_y(t) = \boldsymbol{y}(t) - \hat{\boldsymbol{y}}(t)$ and $\boldsymbol{\xi}'(t) = \boldsymbol{d}_e(t) - \hat{\boldsymbol{d}}_{ev}(t)$.

Since $\boldsymbol{\xi}'(t) \to 0$ with time, we have

$$\dot{\boldsymbol{e}}_x(t) = (\boldsymbol{A} - \boldsymbol{LC} - \boldsymbol{BK}_d\boldsymbol{C})\boldsymbol{e}_x(t). \quad (14)$$

Under Assumption 2, the pair $(\boldsymbol{A} - \boldsymbol{LC},\ \boldsymbol{C})$ is observable.

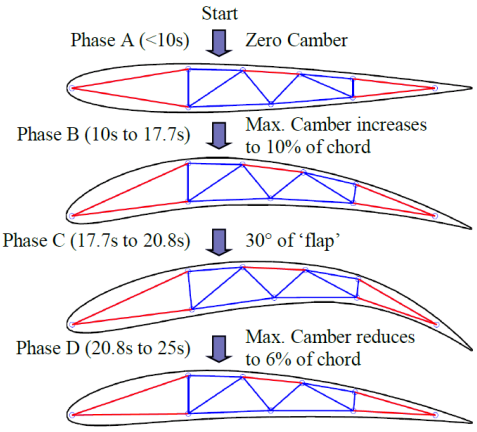

Fig. 3. ATBMW morphing process in a high-lift scenario.

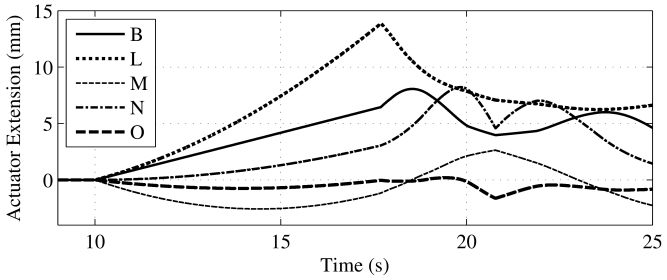

Fig. 4. Extension of actuators for the morphing process in Fig. 3.

Given the duality, one can select $\boldsymbol{K}_v = (\boldsymbol{BK}_d)^{\mathrm{T}}$ that minimizes the performance index

$$J_d = \int_0^\infty \left\{ \boldsymbol{e}_x^{\mathrm{T}}(t)\boldsymbol{Q}_d\boldsymbol{e}_x(t) + \boldsymbol{e}_{dv}^{\mathrm{T}}(t)\boldsymbol{R}_d\boldsymbol{e}_{dv}(t) \right\} dt, \quad (15)$$

with symmetric positive-definite weighting matrices $\boldsymbol{Q}_d$ and $\boldsymbol{R}_d$ of respective sizes $n_x \times n_x$ and $n_y \times n_y$.

As a result,

$$\boldsymbol{K}_d = \boldsymbol{B}^{\dagger}\boldsymbol{K}_v^{\mathrm{T}}, \quad (16)$$

where $\boldsymbol{B}^{\dagger}$ is the Moore-Penrose pseudo inverse of $\boldsymbol{B}$.

IV. Simulations

As mentioned in Section II, ATBMWs in practice can have many variations and actuators are not limited to the electric ones used. To demonstrate the feasibility and practicability of the proposed solution to actuator controller implementation for ATBMW applications, a typical pneumatic cylinder not installed on the presented prototype is also considered for controller evaluation in addition to the five electric miniature linear actuators used. Fig. 3 illustrates a shape morphing process for high lift, with the real-time trajectory for each actuator to follow shown in Fig. 4.

The modeling of a typical pneumatic cylinder follows a commonly adopted form as in [49], in state space with four states, two control inputs, and one measured output (cylinder rod displacement). This nonlinear model with the same parameters as in [49] is used directly as plant dynamics in simulation, while controller design is performed on a linearized form. Despite the existence of two control inputs (denoted by u_{p1}

and u_{p2}) in the model, the control problem is actually an SISO case due to the use of a proportional valve that introduces the constraints of $u_{p1} = u_{p0}$ and $u_{p2} = -u_{p0}$, where u_{p0} denotes the unsigned value of the control effort. Model linearization is performed for the initial conditions of half stroke, zero rod velocity, and 3.3×10^5Pa air pressure in both chambers. The UIE-integrated LQG controller parameters are then obtained by following the systematic procedures provided in Section III.D. Specifically for the subsystem $(\boldsymbol{A}_f, \boldsymbol{B}_f, \boldsymbol{C}_f)$ or $G_f(s)$, a 1^{st}-order low-pass filter is used. The cutoff frequency ω_c is set to 1000 rad/s, which gives an enough bandwidth to cope with most low-frequency disturbances that come from un-modeled dynamics. The resulting UIE-integrated LQG controller has: $K_r = 3.17$, $K_w = -3.16$, $\boldsymbol{K}_x = [3.17 \quad 6.20 \times 10^{-3} \quad 3.12 \times 10^{-9} \quad -2.63 \times 10^{-9}]$, $\boldsymbol{L} = [10.00 \quad 3.06 \times 10^{-2} \quad -6.73 \times 10^3 \quad 6.73 \times 10^3]^{\mathrm{T}}$, $K_d = 1.99 \times 10^{-6}$, and $G_f(s) = \frac{1}{0.001s+1}$.

For comparison, the proportional-integral-derivative (PID) controller is used given the fact that a majority of commercial aircraft wing control surfaces rely on PID controllers. The PID algorithm has a parallel structure with a 1^{st}-order low-pass filter for the derivative term. The setpoint weightings for proportional and derivative terms are both set to 1 for better trajectory tracking [5]. The other parameters are optimally designed and tuned using MATLAB® PID tuner, achieving a 60° phase margin to allow modeling errors or variations in system dynamics. Specifically, the proportional, integral and derivative gains as well as the filter coefficient are $K_P = 6.48 \times 10^{-5}$, $K_I = 5.32 \times 10^{-6}$, $K_D = -3.17 \times 10^{-6}$, and $N = 16.06$, respectively.

The pneumatic actuator (150mm stroke) is assumed being embedded in strut B for a full-scale morphing wing. The corresponding trajectory to follow thus has the same pattern as in Fig. 4, but with its range multiplied by a factor of 7.5. Note that the pneumatic cylinder in the wing assembly is subjected to unknown dynamics resulted from un-modeled inertial, frictional, gravitational and aerodynamic forces as well as the coupling with other active struts, which together are equivalent to a lump exogenous force (in Newton) acting directly on the cylinder rod and simulated by: $F_d = 4.29t + 10\sqrt{t}\sin(0.1\cos(0.63t)t) + 10\cos(0.63t)\sin((0.1t+1)t)$.

As can be seen from the result in Fig. 5, the proposed controller has superior tracking performance over the well-tuned PID algorithm. The pneumatic cylinder rod displacement under the UIE-integrated LQG controller closely follows the target trajectory despite the presence of un-modeled dynamics, while the PID-driven movement significantly deviates from the target trajectory with some oscillation.

In the following, the proposed controller is employed on all the five miniature electric linear actuators of the ATBMW prototype. Actuator dynamics (Category I models) are used for the UIE-integrated LQG controller design directly, parameters of which for each actuator are listed in Table. II. Dynamics unknown to the controllers are introduced into the system by using Category II models for plant dynamics in simulation. No exogenous disturbances are added.

Compensation of un-modeled dynamics is first demonstrated using Actuator B by comparing the UIE-integrated

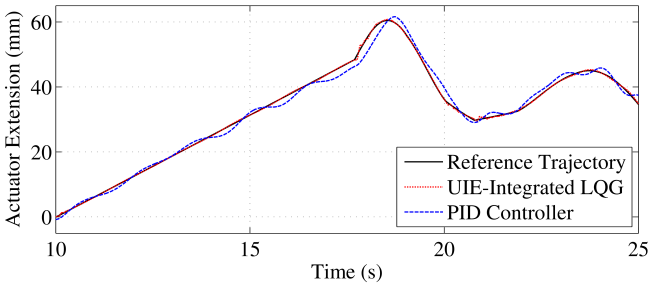

Fig. 5. Trajectory tracking of the pneumatic actuator subjected to un-modeled dynamics.

TABLE II
PARAMETERS OF THE UIE-INTEGRATED LQG CONTROLLER BASED ON ACTUATOR DYNAMICS

	Actuators				
	B	L	M	N	O
K_r	18.71	14.15	14.50	14.15	18.71
K_w	−0.03	−0.03	−0.03	−0.03	−0.03
$\boldsymbol{K}_x$	$\begin{bmatrix}18.71\\0.87\end{bmatrix}^{\mathrm{T}}$	$\begin{bmatrix}14.15\\0.45\end{bmatrix}^{\mathrm{T}}$	$\begin{bmatrix}14.50\\0.50\end{bmatrix}^{\mathrm{T}}$	$\begin{bmatrix}14.16\\0.41\end{bmatrix}^{\mathrm{T}}$	$\begin{bmatrix}18.73\\0.74\end{bmatrix}^{\mathrm{T}}$
K_d	52.12	37.89	37.46	64.06	72.76
$\boldsymbol{L}$	$\begin{bmatrix}223.64\\7.10\end{bmatrix}$	$\begin{bmatrix}223.63\\4.07\end{bmatrix}$	$\begin{bmatrix}223.63\\4.32\end{bmatrix}$	$\begin{bmatrix}223.62\\3.96\end{bmatrix}$	$\begin{bmatrix}223.64\\6.47\end{bmatrix}$
$G_f(s)$	$1/(0.01s+1)$				

LQG controller with a standard LQG scheme of the same parameters. To investigate the impact of un-modeled dynamics, the difference between the tracking trajectories in situations with and without un-modeled dynamics (i.e. relative tracking deviation) is examined. The relative tracking deviation (RTD) under both controllers are plotted in Fig. 6. It can be seen that un-modeled dynamics cause apparent trajectory deviations after 18.5s when using the standard LQG controller. With regard to the UIE-integrated LQG controller, the counteractive compensation effort is generated accordingly in the presence of un-modeled dyanmics (Fig. 7), leaving the LQG component $u_c(t)$ barely affected (Fig. 8). By feeding back proper compensation efforts $\hat{d}_e(t)$ estimated by the UIE, the RTD is effectively reduced as shown in Fig. 6. Under the circumstance with no exogenous disturbances and no un-modeled dynamics, $\hat{d}_e(t)$ simply remains zero as in Fig. 7, which means the corresponding $u_c(t)$ in Fig. 8 is identical to the control effort of a standard LQG controller (without UIE) under the same situation. When un-modeled dynamics are present, there is little change to $u_c(t)$ while $\hat{d}_e(t)$ shows considerable variation, which reveals that the un-modeled dynamics are effectively handled by $\hat{d}_e(t)$. The large magnitude of $\hat{d}_e(t)$ after 18.5s indicates the prescribed nominal LQG control $u_c(t)$ alone is not enough to effectively compensate the un-modeled dynamics, and thus explains the large RTD of the standard LQG controller without UIE (See Fig. 6).

Further comparison with PID is made for all five actuators. The PID design is also based on the actuator dynamics and has a target phase margin over 60°, with the other parameters (as in Table. III) optimally designed and tuned using MATLAB® PID tuner. Tests are divided into two groups:

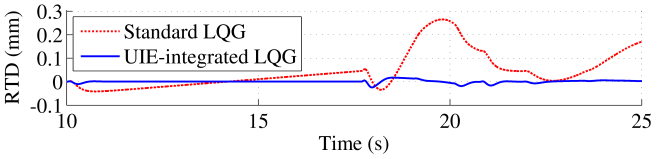

Fig. 6. The relative tracking deviation (RTD) of the standard LQG controller and the UIE-integrated LQG controller in the presence of un-modeled dynamics.

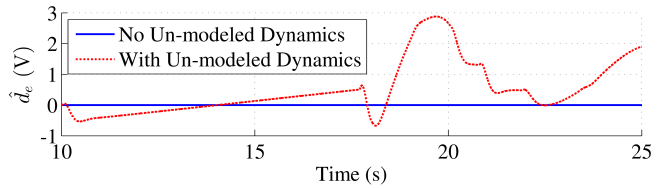

Fig. 7. The estimation $\hat{d}_e(t)$ from the UIE component of the UIE-integrated LQG controller with and without un-modeled dynamics.

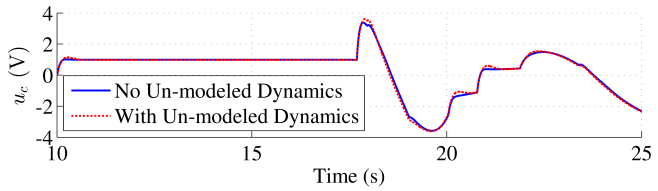

Fig. 8. The control effort $u_c(t)$ from the LQG component of the UIE-integrated LQG controller with and without un-modeled dynamics.

- *Group 1:* Category I models are used as plant dynamics. This simulates the situation that actuators are not assembled onto the wing rib framework.
- *Group 2:* Category II models are used as plant dynamics. It simulates the circumstance that actuators are mounted on the wing rib framework with skin on.

The sampling rate in simulation is set to 0.001s. Results are analyzed in terms of the deviation described by

$$\begin{cases} \alpha_I = \left(\frac{1}{n} \sum_{i=1}^{n} \left(y_I^{(i)} - r^{(i)} \right)^2 \right)^{\frac{1}{2}} \\ \alpha_{II} = \left(\frac{1}{n} \sum_{i=1}^{n} \left(y_{II}^{(i)} - y_I^{(i)} \right)^2 \right)^{\frac{1}{2}}, \end{cases} \tag{17}$$

where

$r^{(i)}$: The i^{th} point of the reference trajectory;
$y_I^{(i)}$: The i^{th} point of Group 1 tracking trajectory;
$y_{II}^{(i)}$: The i^{th} point of Group 2 tracking trajectory;
α_I: Deviation of Group 1 tracking trajectory from the reference trajectory;
α_{II}: Deviation of Group 2 tracking trajectory from Group 1 tracking trajectory;
n: Number of samples.

Comparisons are made according to the normalized relative tracking error (NRTE)

$$\Delta = \frac{\alpha_{II}}{\alpha_I} \times 100\%. \tag{18}$$

TABLE III
PARAMETERS OF THE PID CONTROLLER BASED ON ACTUATOR DYNAMICS

Parameters[a]	Actuators				
	B	L	M	N	O
K_P	10.57	9.76	10.66	9.33	11.81
K_I	0.80	0.81	0.81	0.71	1.00
K_D	0.26	−0.01	0.08	−0.10	0.16
N	18.43	9.51	8.69	90.84	16.75

[a] K_P – Proportional gain; K_I – Integral gain; K_D – Derivative gain; N – Filter coefficient

TABLE IV
NORMALIZED RELATIVE TRACKING ERRORS (NRTE) UNDER THE PID CONTROLLER AND THE UIE-INTEGRATED LQG CONTROLLER IN SIMULATIONS

NRTE (%)	Actuators				
	B	L	M	N	O
Δ_1[a]	64.43%	39.99%	11.60%	53.41%	36.48%
Δ_2[b]	4.87%	3.66%	0.82%	5.78%	4.25%

[a] PID controller based on actuator dynamics
[b] UIE-integrated LQG controller based on actuator dynamics

Given the amount of actuators used and space limit in this paper, tracking results of the actuators are not plotted herein but summarized in Table. IV instead.

As can be seen from the results, un-modeled wing rigid-body dynamics have a substantial impact on actuator responses, resulting in relative tracking errors of considerable extent under the PID controller. However, the UIE-integrated LQG controller has better performance with little difference between Group 2 and Group 1 tracking trajectories in spite of the mismatch between the models used by the controller and those used as plant dynamics.

In summary, the results of controller evaluation for both the pneumatic cylinder and electric linear actuator suggest that the un-modeled wing rigid-body dynamics can be effectively estimated and properly treated with the UIE-integrated LQG controller designed merely using actuator dynamics. The resulting controller performs consistently as designed despite the presence of un-modeled dynamics. Therefore, with the UIE-integrated LQG controller, the difficulties of acquiring sophisticated models of wing rigid-body dynamics for actuator controller design can be avoided. On the contrary, the PID controller designed and tuned purely based on known actuator dynamics is inapplicable for ATBMW applications, since its performance significantly deteriorates after the actuator is assembled onto the wing and subjected to un-modeled dynamics.

V. WIND-TUNNEL EXPERIMENTS

In addition to the induced dynamics from the wing structure, aerodynamic loads during flight is another major factor influencing actuator responses. To investigate the performance of the UIE-integrated LQG controller in flight environment, wind-tunnel tests were conducted.

The overall experiment setup with a wind tunnel is shown in Fig. 9. Though equipped with instruments to measure lift and drag forces generated by the ATBMW prototype, the

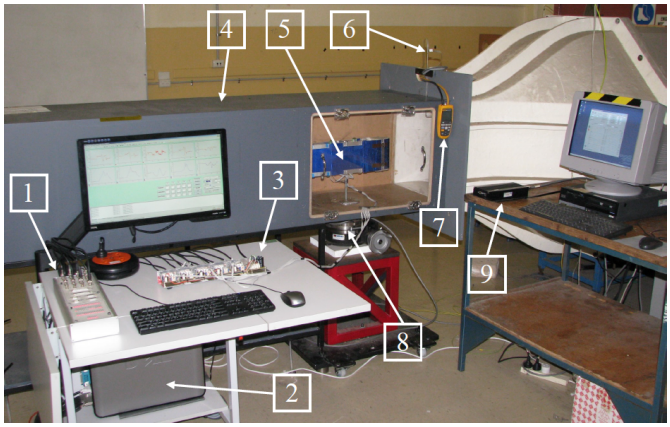

Fig. 9. Wind-tunnel test setup (1, dSPACE® DS1104 R&D controller board; 2, Controller PC; 3, Motor drive board; 4, Testing duct; 5, ATBMW prototype; 6, Pitot tube; 7, Pressure transducer; 8, JR3® multi-axis force-torque sensor; 9, JR3® serial force-torque sensor receiver).

setup is not used to provide force feedbacks to the controller, and hence the aerodynamic loads remain unknown to the controller (which holds true in real-world scenarios). Instead, the measured force data is used to visualize the time-varying dynamic pressure which the ATBMW prototype is subjected to, and to help identify how actuator responses are affected by the aerodynamic forces.

Two scenarios were assumed for experiments:

- *Case 1:* The same high-lift scenario as in Fig. 3.
- *Case 2:* To further investigate the disturbance-rejection capacity of the proposed control scheme, actuators N and O were commanded to flap the trailing edge to generate fluctuating lift forces, while actuator B extended to 6mm and then retracted back to its original length following the trajectory of $6\sin(\pi t/15\ -\pi/2\ )$ within 30 seconds. This scenario simulates the situation that an aircraft is performing tactical maneuvers that require good timing and fast response.

For each scenario, tests were divided into two groups:

- *Group 1:* no wind;
- *Group 2:* room temperature, 8° angle of attack, and 20m/s wind speed.

Each group consisted of three sets of tests:

- *Test A:* Using the UIE-integrated LQG controller designed according to actuator dynamics. Parameters in Table. II were used directly in tests without further tuning.
- *Test B:* Using the UIE-integrated LQG controller designed according to the distributed wing rigid-body dynamics (see parameters in Table. V)
- *Test C:* Using the PID controller designed according to the distributed wing rigid-body dynamics, with parameters optimized and well tuned (Table. VI)

Remark 5: The PID controller based on actuator dynamics (Table. III) was not used in wind tunnel experiments, as it has been shown not able to cope well with un-modeled wing rigid-body dynamics (see Table. IV). On advanced ATBMWs where wing rigid-body dynamics are not available and on-board tuning is difficult, PID control is inapplicable.

TABLE V
PARAMETERS OF THE UIE-INTEGRATED LQG CONTROLLER BASED ON THE DISTRIBUTED WING RIGID-BODY DYNAMICS

	Actuators				
	B	L	M	N	O
K_r	20.00	16.74	15.82	20.00	19.24
K_w	−0.03	−0.03	−0.03	−0.03	−0.03
$\boldsymbol{K}_x$	$\begin{bmatrix}20.16\\0.31\end{bmatrix}^{\mathrm{T}}$	$\begin{bmatrix}16.81\\0.27\end{bmatrix}^{\mathrm{T}}$	$\begin{bmatrix}15.89\\0.35\end{bmatrix}^{\mathrm{T}}$	$\begin{bmatrix}20.02\\0.45\end{bmatrix}^{\mathrm{T}}$	$\begin{bmatrix}19.25\\0.73\end{bmatrix}^{\mathrm{T}}$
K_d	51.63	37.41	33.49	70.77	89.80
$\boldsymbol{L}$	$\begin{bmatrix}223.63\\5.82\end{bmatrix}$	$\begin{bmatrix}223.62\\4.26\end{bmatrix}$	$\begin{bmatrix}223.63\\4.34\end{bmatrix}$	$\begin{bmatrix}223.62\\2.73\end{bmatrix}$	$\begin{bmatrix}223.63\\5.46\end{bmatrix}$
$G_f(s)$	$1/(0.01s+1)$				

TABLE VI
PARAMETERS OF THE PID CONTROLLER BASED ON THE DISTRIBUTED WING RIGID-BODY DYNAMICS

Parameters	Actuators				
	B	L	M	N	O
K_P	18.63	13.29	12.97	15.66	14.94
K_I	1.56	1.13	1.08	1.23	1.15
K_D	−0.29	−0.17	−0.14	−0.21	−0.002
N	9.55	9.73	9.48	8.99	8.81

Every single test was repeated for four times to ensure data consistency, and results are averaged accordingly for subsequent treatments that use (17) and (18). All actuators were ensured to work within their nominal capacity in all tests.

Table. VII summarizes the results from Case 1 tests. The UIE-integrated LQG controllers (Tests A and B) both outperform the PID controller (Test C), with the NRTE several times smaller than that of the PID. Though PID controllers were optimally designed using Category II models and further fine tuned on board, there are nevertheless considerable performance downgrades caused by aerodynamic loads. In addition, the tracking performance of the UIE-integrated LQG controller designed using actuator dynamics is closely comparable to that of its congener based on distributed wing rigid-body dynamics. It is acceptable that actuator O has tracking errors around 11% under the UIE-integrated LQG controllers, given the limited positioning precision of the actuator (see Appendix B for analysis on the influence of actuator precision on experiment results). Two significant implications can be drawn from the results in Table. VII. Firstly, unmeasured aerodynamic loads can be effectively compensated under the UIE-integrated LQG controllers. Secondly, the UIE-integrated LQG controller allows using only the actuator dynamics for controller design in ATBMW applications, with the impact from the un-modeled wing rigid-body dynamics effectively minimized.

In Case 2 tests, the commanded shape morphing of the ATBMW prototype had the lift coefficient in the pattern shown in Fig. 10. The action of actuator B contributed to the major change in the lift while fluctuating waves were caused by the flapping of the trailing edge.

The tracking results under different controllers in Case 2 tests are plotted in Fig. 11 to Fig. 13. We can see from Fig. 13 that the tracking performance of the PID controller is affected by the fluctuating disturbances when the overall lift

TABLE VII
NORMALIZED RELATIVE TRACKING ERRORS (NRTE) UNDER DIFFERENT CONTROLLERS IN TESTS A, B, AND C OF CASE 1

NRTE[a]	Actuators				
	B	L	M	N	O
Δ_A	7.9%	2.7%	5.8%	5.9%	11.3%
Δ_B	7.3%	2.9%	5.5%	4.3%	11.3%
Δ_C	79.1%	16.1%	18.5%	31.8%	65.1%

[a] Subscripts A, B, and C for Δ denote Tests A, B, and C, respectively.

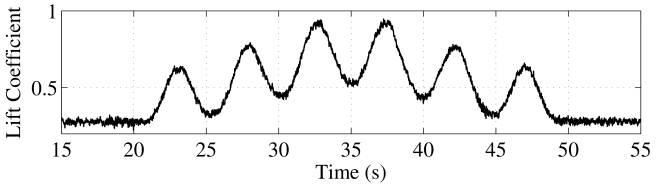

Fig. 10. Lift coefficient of the ATBMW prototype in Case 2 tests.

coefficient is rising ($t < 35$s). The three times of significant trajectory deviations accompany the three consecutive peaks of the lift coefficient. However, such phenomena can be barely seen from the results of the UIE-integrated LQG controller designed using the actuator dynamics (see Fig. 11), which is again closely comparable to its congener design based on the distributed wing rigid-body dynamics (see Fig. 12). Most importantly, it is worth reemphasizing that PID control is inapplicable for advanced ATBMWs as commented in Remark 5. Readers are able to see the results of the PID controller based on wing rigid-body dynamics in this paper is because the presented ATBMW prototype is specially simplified at the cost of sacrificing aerodynamic performance to allow system identification, which is not desired on advanced ATBMWs.

VI. CONCLUSION

The proposed UIE-integrated LQG controller has enhanced tolerance to uncertainties involved in trajectory tracking control of actuators on ATBMWs. Simulations and wind-tunnel experiments on an ATBMW prototype show that with the new control scheme, there is no need to acquire and use wing rigid-body dynamics for controller design, and on-board tuning is no longer required. The UIE-integrated LQG controller can be designed simply using the readily available actuator dynamics, with superior trajectory-tracking capability maintained. This delivers a practical solution to the ATBMW implementation problems associated with the difficulties of modeling the wing rigid-body dynamics and tuning controllers on board. Another significance lies in that the new control scheme proposed in this paper also offers a unified solution to other industrial applications facing considerable impacts from un-modeled dynamics and exogenous disturbances.

APPENDIX A
PROOF OF THEOREM 1

Proof: As discussed in Section III, an equivalent unknown input exists for a system as in (2), and therefore (3) is used in the proof.

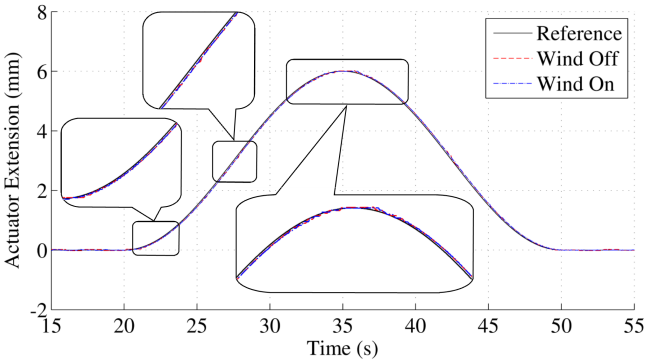

Fig. 11. Actuator B tracking trajectories - Test A of Case 2.

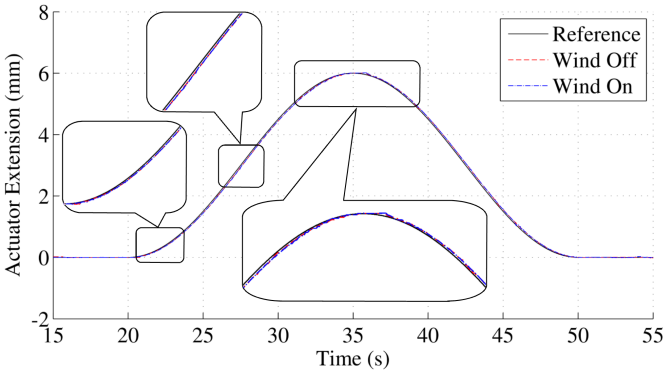

Fig. 12. Actuator B tracking trajectories - Test B of Case 2.

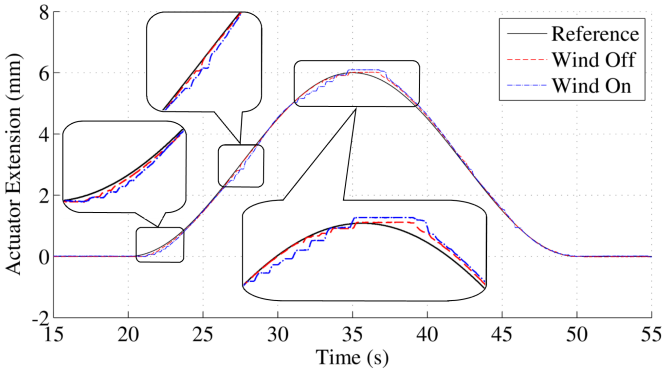

Fig. 13. Actuator B tracking trajectories - Test C of Case 2.

Rewrite (3) in the frequency domain as

$$y(s) = P_n(s)\left[u(s) + d_e(s)\right], \tag{A.1}$$

where $P_n(s)$ is the nominal model of the plant.

Define $G_w(s)$ as the transfer function of the integral action and rewrite (10) as

$$u_c(s) = -\boldsymbol{K}_x\hat{\boldsymbol{x}}(s) - K_w G_w(s)\left[r(s) - y(s)\right] + K_r r(s). \tag{A.2}$$

Substitute (A.2) for $u_c(s)$ in (8), and define $\boldsymbol{G}_{yx}(s)$ as the transfer function matrix from $y(s)$ to $\hat{\boldsymbol{x}}(s)$. When $r(s) = 0$, then

$$\begin{aligned}\hat{\boldsymbol{x}}(s) &= \left(s\boldsymbol{I}_{n_x} - \boldsymbol{A} + \boldsymbol{B}\boldsymbol{K}_x + \boldsymbol{L}\boldsymbol{C}\right)^{-1}\left[\boldsymbol{B}K_w G_w(s) + \boldsymbol{L}\right] y(s) \\ &= \boldsymbol{G}_{yx}(s) y(s).\end{aligned} \tag{A.3}$$

From (5) and (6), we have

$$\hat{d}_{ev}(s) = \boldsymbol{C}_f(s\boldsymbol{I}_{n_f} - \boldsymbol{A}_f)^{-1}\boldsymbol{B}_f\hat{d}_e(s) = G_f(s)\hat{d}_e(s), \quad \text{(A.4)}$$

and

$$\begin{aligned}\hat{d}_e(s) &= [1 - G_f(s)]^{-1}K_d\left[y(s) - \hat{y}(s)\right] \\ &= G_{yd}(s)\left[y(s) - \hat{y}(s)\right], \end{aligned} \quad \text{(A.5)}$$

where $G_{yd}(s)$ is the transfer function from $[y(s) - \hat{y}(s)]$ to $\hat{d}_e(s)$, and $G_f(s)$ is the transfer function of the subsystem $(\boldsymbol{A}_f, \boldsymbol{B}_f, \boldsymbol{C}_f)$.

According to (4), (A.1) to (A.3), and (A.5), the closed-loop system response to $d_e(s)$ is

$$y(s) = P_n(s)[1 + H(s)P_n(s)]^{-1}d_e(s), \quad \text{(A.6)}$$

where

$$H(s) = \boldsymbol{K}_x\boldsymbol{G}_{yx}(s) - K_wG_w(s) + G_{yd}(s)\left[1 - \boldsymbol{C}\boldsymbol{G}_{yx}(s)\right].$$

Since we are able to use (3) as an equivalent of (2), the mechanism of estimating and suppressing unknown inputs can be revealed by the relation between the equivalent unknown input $d_e(t)$ and the system output $y(t)$.

Equation (A.6) indicates that, under a given $P_n(s)$ and a properly designed LQG controller, minimizing the term of $\|P_n(s)[1 + H(s)P_n(s)]^{-1}\|_\infty$ can effectively suppress the influences from unknown inputs. In other words, if an $H(s)$ exists so that $\|P_n(s)[1 + H(s)P_n(s)]^{-1}\|_\infty$ is sufficiently small, then an estimate of adequate accuracy for the equivalent unknown input can be obtained, and feeding this estimate back into the system can effectively counteract the actual unknown inputs, alleviating disturbances.

This can be achieved by proper design of the subsystem $(\boldsymbol{A}_f, \boldsymbol{B}_f, \boldsymbol{C}_f)$. For a majority of servo systems in which most disturbances are from low-frequency sources, a viable solution requires $G_f(j\omega)$ to be approximately equal to but less than 1 for $\omega \in [0, \omega_c]$. As a result, $y(s) \approx 0$ in (A.6) for any finite $d_e(s)$ with frequency lower than ω_c. This means, though $\|P_n(s)[1 + H(s)P_n(s)]^{-1}\|_\infty$ cannot be minimized ideally for $\omega \in [0, \infty)$, the introduction of a low-pass filter suffices when the frequency of unknown inputs to be suppressed are below ω_c. It is worth emphasizing that the design of $(\boldsymbol{A}_f, \boldsymbol{B}_f, \boldsymbol{C}_f)$ is not limited to the low-pass filter as discussed herein, but flexible for various situations, and the most suitable configuration depends on the application under consideration.

According to equations from (3) to (6),

$$\begin{aligned}\dot{\boldsymbol{x}}(t) &= \boldsymbol{A}\boldsymbol{x}(t) + \boldsymbol{B}u_c(t) + \boldsymbol{B}[d_e(t) - \hat{d}_e(t)] \\ &= \boldsymbol{A}\boldsymbol{x}(t) + \boldsymbol{B}u_c(t) - \boldsymbol{B}\boldsymbol{C}_f\boldsymbol{x}_f(t) \\ &\quad - \boldsymbol{B}K_d\boldsymbol{C}\left[\boldsymbol{x}(t) - \hat{\boldsymbol{x}}(t)\right] + \boldsymbol{B}d_e(t). \end{aligned} \quad \text{(A.7)}$$

Subtract (8) from (A.7), and let $\boldsymbol{e}_x(t) = \boldsymbol{x}(t) - \hat{\boldsymbol{x}}(t)$, then

$$\begin{aligned}\dot{\boldsymbol{e}}_x(t) &= (\boldsymbol{A} - \boldsymbol{L}\boldsymbol{C} - \boldsymbol{B}K_d\boldsymbol{C})\,\boldsymbol{e}_x(t) \\ &\quad - \boldsymbol{B}\boldsymbol{C}_f\boldsymbol{x}_f(t) + \boldsymbol{B}d_e(t). \end{aligned} \quad \text{(A.8)}$$

Substituting (10) for $u_c(t)$ in (A.7) with some manipulation using $\hat{\boldsymbol{x}}(t) = \boldsymbol{x}(t) - \boldsymbol{e}_x(t)$ yields

$$\begin{aligned}\dot{\boldsymbol{x}}(t) &= (\boldsymbol{A} - \boldsymbol{B}\boldsymbol{K}_x)\,\boldsymbol{x}(t) - \boldsymbol{B}K_wx_w(t) \\ &\quad + (\boldsymbol{B}\boldsymbol{K}_x - \boldsymbol{B}K_d\boldsymbol{C})\,\boldsymbol{e}_x - \boldsymbol{B}\boldsymbol{C}_f\boldsymbol{x}_f(t) \\ &\quad + \boldsymbol{B}K_rr(t) + \boldsymbol{B}d_e(t). \end{aligned} \quad \text{(A.9)}$$

From (5) and (6),

$$\begin{aligned}\dot{\boldsymbol{x}}_f(t) &= \boldsymbol{A}_f\boldsymbol{x}_f(t) + \boldsymbol{B}_f\left\{\hat{d}_{ev} + K_d\left[y(t) - \hat{y}(t)\right]\right\} \\ &= (\boldsymbol{A}_f + \boldsymbol{B}_f\boldsymbol{C}_f)\,\boldsymbol{x}_f(t) + \boldsymbol{B}_fK_d\boldsymbol{C}\boldsymbol{e}_x(t). \end{aligned} \quad \text{(A.10)}$$

Arranging (9), (A.8), (A.9), and (A.10) in matrix form with appropriate matrix partitioning yields

$$\dot{\boldsymbol{z}}(t) = \begin{bmatrix}\bar{\boldsymbol{A}}_{11} & \bar{\boldsymbol{A}}_{12} \\ \boldsymbol{0} & \bar{\boldsymbol{A}}_{22}\end{bmatrix}\boldsymbol{z}(t) + \bar{\boldsymbol{B}}_rr(t) + \bar{\boldsymbol{B}}_dd_e(t), \quad \text{(A.11)}$$

where

$$\boldsymbol{z}(t) = [\boldsymbol{x}(t) \quad x_w(t) \quad e_x(t) \quad \boldsymbol{x}_f(t)]^{\mathrm{T}},$$

$$\bar{\boldsymbol{A}}_{11} = \begin{bmatrix}\boldsymbol{A} - \boldsymbol{B}\boldsymbol{K}_x & -\boldsymbol{B}K_w \\ -\boldsymbol{C} & 0\end{bmatrix},$$

$$\bar{\boldsymbol{A}}_{12} = \begin{bmatrix}\boldsymbol{B}\boldsymbol{K}_x - \boldsymbol{B}K_d\boldsymbol{C} & -\boldsymbol{B}\boldsymbol{C}_f \\ 0 & 0\end{bmatrix},$$

$$\bar{\boldsymbol{A}}_{22} = \begin{bmatrix}\boldsymbol{A} - \boldsymbol{L}\boldsymbol{C} - \boldsymbol{B}K_d\boldsymbol{C} & -\boldsymbol{B}\boldsymbol{C}_f \\ \boldsymbol{B}_fK_d\boldsymbol{C} & \boldsymbol{A}_f + \boldsymbol{B}_f\boldsymbol{C}_f\end{bmatrix},$$

$$\bar{\boldsymbol{B}}_r = [\boldsymbol{B}K_r \quad 1 \quad 0 \quad 0]^{\mathrm{T}},$$

$$\bar{\boldsymbol{B}}_d = [\boldsymbol{B} \quad 0 \quad \boldsymbol{B} \quad 0]^{\mathrm{T}},$$

and $\boldsymbol{0}$ is a null matrix.

The characteristic equation associated with (A.11) is

$$\det\left(\bar{\boldsymbol{D}}_1\right) \cdot \det\left(\bar{\boldsymbol{D}}_2\right) \cdot \det\left(\bar{\boldsymbol{D}}_3\right) = 0, \quad \text{(A.12)}$$

where

$$\bar{\boldsymbol{D}}_1 = \begin{bmatrix}s\boldsymbol{I} - (\boldsymbol{A} - \boldsymbol{B}\boldsymbol{K}_x) & \boldsymbol{B}K_w \\ \boldsymbol{C} & s\end{bmatrix},$$

$$\bar{\boldsymbol{D}}_2 = s\boldsymbol{I} - (\boldsymbol{A} - \boldsymbol{L}\boldsymbol{C} - \boldsymbol{B}K_d\boldsymbol{C}),$$

and

$$\bar{\boldsymbol{D}}_3 = s\boldsymbol{I} - \boldsymbol{A}_f - \boldsymbol{B}_f\left(1 - K_d\boldsymbol{C}\bar{\boldsymbol{D}}_2^{-1}\boldsymbol{B}\right)\boldsymbol{C}_f.$$

If the system as in (2) with any initial condition $\boldsymbol{x}(t_0)$ is stabilized with full-state feedback (no state observer and no UIE) when $\boldsymbol{d}(t) = 0$, it is a case of linear-quadratic optimal control with integral action, the characteristic equation of which is

$$\det\left(\bar{\boldsymbol{D}}_1\right) = 0. \quad \text{(A.13)}$$

Note that the roots of (A.13), which lie in the left half-plane, are also part of the roots of (A.12). If a proper $\boldsymbol{L} \in \mathbb{R}^{n_x \times 1}$ and $K_d \in \mathbb{R}^+$ are selected such that $(\boldsymbol{A} - \boldsymbol{L}\boldsymbol{C} - \boldsymbol{B}K_d\boldsymbol{C})$ is stable, and if $(\boldsymbol{A}_f, \boldsymbol{B}_f, \boldsymbol{C}_f)$ satisfies condition (a), then all roots of (A.12) are in the left half-plane. Under Assumption 2 in Section III, such an $\boldsymbol{L}$ and K_d exist.

Based on the absolute stability discussed, the relative stability needs to be considered in the presence of un-modeled dynamics $M(s)$. As illustrated in Fig. 14, the relation between the nominal plant model $P_n(s)$ and the actual process $P(s)$ is

$$P(s) = P_n(s)\left[1 + M(s)\right]. \quad \text{(A.14)}$$

An equivalent block diagram depiction for the system in Fig. 14 is given in Fig. 15. According to the small-gain

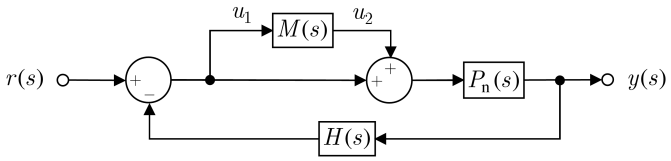

Fig. 14. Un-modeled dynamics $M(s)$ in the closed-loop system.

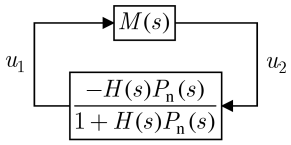

Fig. 15. Equivalent block diagram depiction of the closed-loop system with un-modeled dynamics $M(s)$.

TABLE VIII
NORMALIZED RELATIVE TRACKING ERRORS (NRTE) IN CASE 1 TESTS DUE TO ACTUATOR PRECISION LIMITATION

NRTE[a]	Actuators				
	B	L	M	N	O
Δ'_A	3.4%	2.3%	5.0%	3.3%	11.0%
Δ'_B	3.3%	2.4%	4.7%	3.1%	10.9%
Δ'_C	3.8%	2.6%	5.2%	3.6%	11.2%

[a] Subscripts A, B, and C for Δ' denote Tests A, B, and C, respectively.

theorem [50], the closed-loop system remains stable in the presence of $M(s)$ if

$$|M(j\omega)|\left|\frac{H(j\omega)P_n(j\omega)}{1+H(j\omega)P_n(j\omega)}\right|<1,\ \forall\omega\in[0,+\infty)\,, \quad \text{(A.15)}$$

or equivalently,

$$|M(j\omega)|<\left|1+\frac{1}{H(j\omega)P_n(j\omega)}\right|,\ \forall\omega\in[0,+\infty)\,. \quad \text{(A.16)}$$

This completes the proof. ■

APPENDIX B
ANALYSIS OF THE INFLUENCE OF ACTUATOR PRECISION ON EXPERIMENT RESULTS

The actuators used on the prototype have a linear positioning precision of 0.1mm as claimed by the manufacturer. In order to evaluate the influence of the actuator precision on experiment results, any two of the four runs (i.e. $4!/(4-2)!=12$ pairs in total in every single test) are compared by following the same treatment using (17) and (18), with results averaged and listed in Table. VIII. As can be seen in Table. VIII, the normalized relative tracking errors (NRTE) of each actuator caused by the limited positioning precision are generally consistent regardless of the different controllers used. Associated with the actuator precision, reference trajectories also have an impact on the NRTE. For a given positioning precision, a smaller trajectory range results in relatively coarser trajectory discretization, thus causing larger NRTE.

REFERENCES

[1] D. Coutu, V. Brailovski, P. Terriault, M. Mamou, Y. Mébarki, and É. Laurendeau, "Lift-to-drag ratio and laminar flow control of a morphing laminar wing in a wind tunnel," *Smart Mater. Struct.*, vol. 20, no. 3, 035019. Feb. 2011.
[2] F. Austin, M. J. Rossi, W. V. Nostrand, G. Knowles, and A. Jameson, "Static shape control for adaptive wings," *AIAA J.*, vol. 32, no. 9, pp. 1895–1901, Sep. 1994.
[3] D. Baker and M. I. Friswell, "Determinate structures for wing camber control," *Smart Mater. Struct.*, vol. 18, no. 3, 035014. Feb. 2009.
[4] Y. Liu, H. Du, L. Liu, and J. Leng, "Shape memory polymers and their composites in aerospace applications: A review," *Smart Mater. Struct.*, vol. 23, no. 2, 023001. Jan. 2014.
[5] K. J. Åström and T. Hägglund, *Advanced PID Control*. Research Triangle Park, NC: Instrumentation, Systems, and Automation Society, 2006.
[6] T. Schuhmann, W. Hofmann, and R. Werner, "Improving operational performance of active magnetic bearings using Kalman filter and state feedback control," *IEEE Trans. Ind. Electron.*, vol. 59, no. 2, pp. 821–829, Feb. 2012.
[7] L. Chen, F. He, and K. Sammut, "Vibration suppression of a principal parametric resonance," *J. Vib. Control*, vol. 15, no. 3, pp. 439–463, Mar. 2009.
[8] G. Andrikopoulos, G. Nikolakopoulos, and S. Manesis, "Advanced nonlinear PID-based antagonistic control for pneumatic muscle actuators," *IEEE Trans. Ind. Electron.*, vol. 61, no. 12, pp. 6926–6937, Dec. 2014.
[9] B. Zhao, B. Xian, Y. Zhang, and X. Zhang, "Nonlinear robust adaptive tracking control of a quadrotor UAV via immersion and invariance methodology," *IEEE Trans. Ind. Electron.*, vol. 62, no. 5, pp. 2891–2902, May. 2015.
[10] S. G. Dietz and C. W. Scherer, "Robust output feedback control against disturbance filter uncertainty described by dynamic integral quadratic constraints," *Int. J. Robust Nonlin.*, vol. 20, no. 17, pp. 1903–1919, Nov. 2010.
[11] J. Yang, Y. Zhu, W. Yin, C. Hu, K. Yang, and H. Mu, "LFT structured uncertainty modeling and robust loop-shaping controller optimization for an ultraprecision positioning stage," *IEEE Trans. Ind. Electron.*, vol. 61, no. 12, pp. 7013–7025, Dec. 2014.
[12] M. B. Ketzer and C. B. Jacobina, "Sensorless control technique for PWM rectifiers with voltage disturbance rejection and adaptive power factor," *IEEE Trans. Ind. Electron.*, vol. 62, no. 2, pp. 1140–1151, Feb. 2015.
[13] M. Mohammadzaheri and L. Chen, "Double-command fuzzy control of a nonlinear CSTR," *Korean J. Chem. Eng.*, vol. 27, no. 1, pp. 19–31, Jan. 2010.
[14] M. Mohammadzaheri and L. Chen, "Intelligent predictive control of a model helicopter's yaw angle," *Asian J. Control*, vol. 12, no. 6, pp. 667–679, Nov. 2010.
[15] J.-H. She, X. Xin, and Y. Pan, "Equivalent-input-disturbance approach — analysis and application to disturbance rejection in dual-stage feed drive control system," *IEEE-ASME Trans. Mech.*, vol. 16, no. 2, pp. 330–340, Apr. 2011.
[16] C. Mitsantisuk, K. Ohishi, and S. Katsura, "Control of interaction force of twin direct-drive motor system using variable wire rope tension with multisensor integration," *IEEE Trans. Ind. Electron.*, vol. 59, no. 1, pp. 498–510, Jan. 2012.
[17] S.-H. Lee, H. J. Kang, and C. C. Chung, "Robust fast seek control of a servo track writer using a state space disturbance observer," *IEEE Trans. Contr. Syst. T.*, vol. 20, no. 2, pp. 346–355, Mar. 2012.
[18] K. Erenturk, "Fractional-order $PI^{\lambda}D^{\mu}$ and active disturbance rejection control of nonlinear two-mass drive system," *IEEE Trans. Ind. Electron.*, vol. 60, no. 9, pp. 3806–3813, Sep. 2013.
[19] T. S. Chandar and S. E. Talole, "Improving the performance of UDE-based controller using a new filter design," *Nonlinear Dynam.*, vol. 77, no. 3, pp. 753–768, Aug. 2014.
[20] H. Tang and Y. Li, "Development and active disturbance rejection control of a compliant micro-/nanopositioning piezostage with dual mode," *IEEE Trans. Ind. Electron.*, vol. 61, no. 3, pp. 1475–1492, Mar. 2014.
[21] S. Zheng, B. Han, and L. Guo, "Composite hierarchical antidisturbance control for magnetic bearing system subject to multiple external disturbances," *IEEE Trans. Ind. Electron.*, vol. 61, no. 12, pp. 7004–7012, Dec. 2014.
[22] X. Chang, Y. Li, W. Zhang, N. Wang, and W. Xue, "Active disturbance rejection control for a flywheel energy storage system," *IEEE Trans. Ind. Electron.*, vol. 62, no. 2, pp. 991–1001, Feb. 2015.

[23] K. Ohishi, M. Nakao, K. Ohnishi, and K. Miyachi, "Microprocessor-controlled DC motor for load-insensitive position servo system," *IEEE Trans. Ind. Electron.*, vol. IE-34, no. 1, pp. 44–49, Feb. 1987.
[24] W. Lu, K. Zhou, D. Wang, and M. Cheng, "A generic digital nk±m-order harmonic repetitive control scheme for PWM converters," *IEEE Trans. Ind. Electron.*, vol. 61, no. 3, pp. 1516–1527, Mar. 2014.
[25] S. Li, J. Yang, W.-H. Chen, and X. Chen, "Generalized extended state observer based control for systems with mismatched uncertainties," *IEEE Trans. Ind. Electron.*, vol. 59, no. 12, pp. 4792–4802, Dec. 2012.
[26] A. A. Godbole, J. P. Kolhe, and S. E. Talole, "Performance analysis of generalized extended state observer in tackling sinusoidal disturbances," *IEEE Trans. Contr. Syst. T.*, vol. 21, no. 6, pp. 2212–2223, Nov. 2013.
[27] H. Kim, H. Shim, and N. H. Jo, "Adaptive add-on output regulator for rejection of sinusoidal disturbances and application to optical disc drives," *IEEE Trans. Ind. Electron.*, vol. 61, no. 10, pp. 5490–5499, Oct. 2014.
[28] J. Yang, S. Li, C. Sun, and L. Guo, "Nonlinear-disturbance-observer-based robust flight control for airbreathing hypersonic vehicles," *IEEE Trans. Aerosp. Electron. Syst.*, vol. 49, no. 2, pp. 1263–1275, Apr. 2013.
[29] X. Wei and N. Chen, "Composite hierarchical anti-disturbance control for nonlinear systems with DOBC and fuzzy control," *Int. J. Robust Nonlin.*, vol. 24, no. 2, pp. 362–373, Jan. 2014.
[30] M. Hou and P. C. Müller, "Design of observers for linear systems with unknown inputs," *IEEE Trans. Automat. Contr.*, vol. 37, no. 6, pp. 871–875, Jun. 1992.
[31] D. G. Luenberger, "Observing the state of a linear system," *IEEE Trans. Mil. Electron.*, vol. 8, no. 2, pp. 74–80, Apr. 1964.
[32] Y.-X. Wang, D.-H. Yu, and Y.-B. Kim, "Robust time-delay control for the DC–DC boost converter," *IEEE Trans. Ind. Electron.*, vol. 61, no. 9, pp. 4829–4837, Sep. 2014.
[33] M. Corless and J. Tu, "State and input estimation for a class of uncertain systems," *Automatica*, vol. 34, no. 6, pp. 757–764, Jun. 1998.
[34] C.-S. Liu and H. Peng, "Disturbance observer based tracking control," *J. Dyn. Syst.-Trans. ASME*, vol. 122, no. 2, pp. 332–335, Jun. 2000.
[35] Y. Xiong and M. Saif, "Unknown disturbance inputs estimation based on a state functional observer design," *Automatica*, vol. 39, no. 8, pp. 1389–1398, Aug. 2003.
[36] K.-S. Kim and K.-H. Rew, "Reduced order disturbance observer for discrete-time linear systems," *Automatica*, vol. 49, no. 4, pp. 968–975, Apr. 2013.
[37] S. Li, J. Li, and Y. Mo, "Piezoelectric multimode vibration control for stiffened plate using ADRC-based acceleration compensation," *IEEE Trans. Ind. Electron.*, vol. 61, no. 12, pp. 6892–6902, Dec. 2014.
[38] J.-H. She, M. Fang, Y. Ohyama, H. Hashimoto, and M. Wu, "Improving disturbance-rejection performance based on an equivalent-input-disturbance approach," *IEEE Trans. Ind. Electron.*, vol. 55, no. 1, pp. 380–389, Jan. 2008.
[39] R.-J. Liu, M. Wu, G.-p. Liu, J. She, and C. Thomas, "Active disturbance rejection control based on an improved equivalent-input-disturbance approach," *IEEE-ASME Trans. Mech.*, vol. 18, no. 4, pp. 1410–1413, Aug. 2013.
[40] K. Ohnishi, "New development of servo technology in mechatronics," *IEEJ Trans. Ind. Applic.*, vol. 107-D, no. 1, pp. 83–86, 1987.
[41] T. Umeno and Y. Hori, "Robust speed control of DC servomotors using modern two degrees-of-freedom controller design," *IEEE Trans. Ind. Electron.*, vol. 38, no. 5, pp. 363–368, Oct. 1991.
[42] T. Umeno, T. Kaneko, and Y. Hori, "Robust servosystem design with two degrees of freedom and its application to novel motion control of robot manipulators," *IEEE Trans. Ind. Electron.*, vol. 40, no. 5, pp. 473–485, Oct. 1993.
[43] Y. Choi, K. Yang, W. K. Chung, H. R. Kim, and I. H. Suh, "On the robustness and performance of disturbance observers for second-order systems," *IEEE Trans. Automat. Contr.*, vol. 48, no. 2, pp. 315–320, Feb. 2003.
[44] S. M. Shahruz, "Active vibration suppression in multi-degree-of-freedom systems by disturbance observers," *J. Vib. Control*, vol. 15, no. 8, pp. 1207–1228, Aug. 2009.
[45] C. Du, H. Li, C. K. Thum, F. L. Lewis, and Y. Wang, "Simple disturbance observer for disturbance compensation," *IET Control Theory Appl.*, vol. 4, no. 9, pp. 1748–1755, Sep. 2010.
[46] L. Ljung, *System Identification: Theory for the User*, 2nd ed. Upper Saddle River, NJ: Prentice-Hall PTR, 1999.
[47] W. S. Levine, Ed., *The Control Handbook*. Boca Raton, Fl: CRC Press, 1995.
[48] B. D. O. Anderson and J. B. Moore, *Optimal Control: Linear Quadratic Methods*. Englewood Cliffs, NJ: Prentice-Hall, 1990.
[49] N. Gulati and E. J. Barth, "A globally stable, load-independent pressure observer for the servo control of pneumatic actuators," *IEEE/ASME Trans. Mechatron.*, vol. 14, no. 3, pp. 295–306, Jun. 2009.
[50] M. Vidyasagar, *Nonlinear Systems Analysis*. Englewood Cliffs, NJ: Prentice-Hall, 1978.

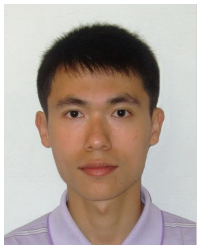

Difan Tang (S'15) received the B.Eng. degree in mechanical engineering and automation from South China University of Technology, China, in 2006, the M.Sc. degree in mechanical engineering from the University of Sheffield, U.K., in 2007, the M.Eng.Sc. degree in mechatronics from the University of Adelaide, Australia, in 2012. He is currently working toward the Ph.D. degree in mechatronics at the University of Adelaide, Australia.

He was an engineer at ZWCAD Software Co., Ltd., China, from 2008 to 2009. His current research interests include adaptive, nonlinear and optimal control for smart structures.

Lei Chen (M'00) received the B.Eng. degree in electrical and electronic engineering and the M.Eng. degree in electrical and computer engineering from Huazhong University of Science and Technology, Wuhan, China, and the Ph.D. degree in mechatronics engineering from Flinders University, Adelaide, Australia, in 2004.

From 2004 he was a Lecturer and then Senior Lecturer with the School of Mechanical Engineering, University of Adelaide, South Australia. His research interests include the development of nonlinear control for smart materials and structures, robotics, and artificial intelligent systems for HVAC applications.

Dr. Chen is a member of IEEE and ASHRAE.

Eric Hu received the B.Eng. degree in mechanical engineering from Zhejiang University, China, in 1984, the M.Eng. degree in energy technology from Beijing Normal College, China, in 1987, and the Ph.D. degree in energy technology from Asian Institute of Technology, Thailand, in 1992.

He worked as a lecturer and senior lecturer in thermodynamics and fluid mechanics at School of Engineering, Monash University, Melbourne, Australia, from 1993 to 1999 when he joined the School of Engineering and Technology at Deakin University, Geelong, Australia. He starts with the School of Mechanical Engineering at the University of Adelaide, Adelaide, Australia, as Associate Professor in sustainable energy engineering, in 2009. He has been working in energy engineering areas, including energy efficiencies for industrial process, solar thermal applications eg. heating, cooling and power generation, CO2 emission reduction for power stations and low energy desalination etc. He has won over $2.5m in research grant and published over 150 academic papers in Australia.

Zhao Feng Tian received the B.Eng. degree in thermal engineering from Shanghai Jiaotong University, China, in 1997, the M.Eng.Sc. degree in mechanical engineering from the University of New South Wales, Australia, in 2002, and the Ph.D. degree in mechanical engineering from RMIT University, Australia, in 2007.

He was a postdoctoral fellow with the devision of Mathematics, Informatics and Statistics (CMIS) of Commonwealth Scientific and Industrial Research Organization (CSIRO), Australia, from 2007 to 2010. Currently he is a senior lecturer in the School of Mechanical Engineering at the University of Adelaide, Australia. His research interests include fluid dynamics, heat transfer, computational fluid dynamics (CFD), and CFD modeling of engineering combustion.